Cerebral Cortex, 2017; 1–11

doi: 10.1093/cercor/bhx322
Original Article

ORIGINAL ARTICLE

Longitudinal Functional Brain Mapping in Supernormals

Xixi Wang[1], Ping Ren[2], Timothy M. Baran[1,3], Rajeev D. S. Raizada[4], Mark Mapstone[5], Feng Lin[2,4,6,7], for the Alzheimer's Disease Neuroimaging Initiative[*]

[1]Department of Biomedical Engineering, University of Rochester, Rochester, NY 14627, USA, [2]School of Nursing, University of Rochester Medical Center, Rochester, NY 14642, USA, [3]Department of Imaging Sciences, University of Rochester, Rochester, NY 14642, USA, [4]Department of Brain and Cognitive Sciences, University of Rochester, Rochester, NY 14627, USA, [5]Department of Neurology, University of California-Irvine, Irvine, CA 92697, USA, [6]Department of Neuroscience, University of Rochester Medical Center, Rochester, NY 14642, USA and [7]Department of Psychiatry, University of Rochester Medical Center, Rochester, NY 14642, USA

Address correspondence to Feng Vankee Lin, 601 Elmwood Ave, Rochester, NY 14642, USA. Email: vankee_lin@urmc.rochester.edu

[*]Data used in preparation of this article were obtained from the Alzheimer's Disease Neuroimaging Initiative (ADNI) database (adni.loni.usc.edu). As such, the investigators within the ADNI contributed to the design and implementation of ADNI and/or provided data but did not participate in analysis or writing of this report. A complete listing of ADNI investigators can be found at: http://adni.loni.usc.edu

Abstract

Prevention of age-related cognitive decline is an increasingly important topic. Recently, increased attention is being directed at understanding biological models of successful cognitive aging. Here, we examined resting-state brain regional low-frequency oscillations using functional magnetic resonance imaging in 19 older adults with excellent cognitive abilities (Supernormals), 28 older adults with normative cognition, 57 older adults with amnestic mild cognitive impairment, and 26 with Alzheimer's disease. We identified a "Supernormal map", a set of regions whose oscillations were resistant to the aging-associated neurodegenerative process, including the right fusiform gyrus, right middle frontal gyrus, right anterior cingulate cortex, left middle temporal gyrus, left precentral gyrus, and left orbitofrontal cortex. The map was unique to the Supernormals, differentiated this group from cognitive average-ager comparisons, and predicted a 1-year change in global cognition (indexed by the Montreal Cognitive Assessment scores, adjusted $R^2 = 0.68$). The map was also correlated to Alzheimer's pathophysiological features (beta-amyloid/pTau ratio, adjusted $R^2 = 0.66$) in participants with and without cognitive impairment. These findings in phenotypically successful cognitive agers suggest a divergent pattern of brain regions that may either reflect inherent neural integrity that contributes to Supernormals' cognitive success, or alternatively indicate adaptive reorganization to the demands of aging.

Key words: Alzheimer's pathophysiology, beta-amyloid/pTau ratio, longitudinal, resting-state functional MRI, Supernormal

Introduction

Cognitive aging trajectories are most often characterized by a gradual decline of cognitive performance commonly beginning in the fifth or sixth decade of life (Ronnlund et al. 2005). Individual trajectories are unique with regard to which cognitive abilities are affected and to what degree, but most

age-related cognitive changes may be related to a fundamental deterioration of information transfer across widespread brain networks (Salthouse 2009; Reuter-Lorenz and Park 2010). These distributed brain networks can be disrupted as a consequence of regionally specific structural or functional changes, and emergent properties of the networks will be affected accordingly (Andrews-Hanna et al. 2007). However, it is unclear whether successful cognitive aging may rely on the individual's ability to initially resist (reserve) or eventually adapt to regional brain changes (compensation) (Stern et al. 2008; Park and Reuter-Lorenz 2009; Gutchess 2014).

Inspired by early literature on successful aging (Baltes and Carstensen 1996; Schulz and Heckhausen 1996), there has been a growing body of work specifically emphasizing the biological models of successful cognitive aging (Lindenberger 2014). In one instantiation, "Supernormals" are a unique group of individuals who demonstrate above-average to superior cognitive performance compared to age- and education-matched cognitively average-for-age older adults (i.e., average-agers) (Mapstone et al. 2016; Lin et al. 2017a). In other definitions, Super-agers demonstrate comparable performance to younger or middle-aged individuals (Pudas et al. 2013; Rogalski et al. 2013; Gefen et al. 2014, 2015; Sun et al. 2016; Bott et al. 2017). In both definitions, these cognitively superior individuals show preserved genetic and biochemical relative to those in both normal and abnormal aging processes. Specifically, these individuals exhibit low frequency of apolipoprotein E allele 4 (APOE4) carriers (Rogalski et al. 2013; Lin et al. 2017b), low oxidative stress burden (Mapstone et al. 2016), and low levels of amyloid or tau deposition (Rogalski et al. 2013; Lin et al. 2017a).

More recent efforts are being made to fully understand the neural integrity of Supernormals. A recent longitudinal study revealed slower brain atrophy rates in Supernormals compared to average-agers (Cook et al. 2017), while other emerging literatures seem to reach a consensus on testing the role of maintaining multiple anterior and posterior regions in Supernormals. Among the brain structure literature, compared to average-agers or younger adults, Supernormals showed greater cortical thickness or volume in the anterior cingulate cortex (Harrison et al. 2012; Rogalski et al. 2013; Gefen et al. 2015), multiple regions within the default mode network (Sun et al. 2016), the corpus callosum (Bott et al. 2017), and the medial temporal lobe (Rosano et al. 2012). Among the brain function literature, Persson et al.'s longitudinal study suggested the functional stability of the medial temporal lobe in maintaining memory performance in aging (Persson et al. 2012). In our previous cross-sectional work, Supernormals tended to have strengthened networks among posterior regions (e.g., left superior/middle temporal gyrus) or between posterior and anterior regions (e.g., anterior cingulate cortex and right middle frontal gyrus) but weakened networks between anterior regions (Lin et al. 2017a). These structural and functional imaging literatures seem to agree on the importance of maintaining the "youth-like" posterior-oriented brain regions for successful cognitive aging (Nyberg et al. 2012; Lindenberger 2014), or the emphasis on posterior region-oriented neural reserve on driving cognitive maintenance and brain health (Stern et al. 2008), while contrast with the view on a typical cognitive aging process—relying on anterior regions to compensate for the functional loss of posterior regions (Park and Reuter-Lorenz 2009).

Meanwhile, structural measures have been shown more relevant to cognitive decline than cognitive maintenance over time (Burgmans et al. 2009) while functional capacity of large-scale brain networks seems to be more vulnerable to aging than structure itself, at least among those without cognitive deficits (Pudas et al. 2013; Fjell et al. 2016). Hence, to further validate the findings concerning the roles of anterior versus posterior regions in cognitive maintenance, we proposed to conduct a data-driven longitudinal study focusing on neural functional integrity of Supernormals. We hypothesized that Supernormals maintain a unique set of brain regions, whose functional integrity would be resistant to the aging process by supporting the longitudinal stability of superior cognitive performance and fighting against aging-related neuropathological changes. Specifically, compared to the average-agers, the neural reserve-related posterior regions may be more active in Supernormals while neural compensation-related anterior regions may be less active.

To examine this hypothesis, we first developed a "Supernormal map" based on longitudinally stable neural patterns in Supernormals. We applied a machine-learning-based multivariate pattern analysis approach called "searchlight analysis" to examine the longitudinal difference in neural patterns derived from amplitude of low-frequency fluctuation (ALFF) of the resting-state functional MRI (rs-fMRI), between Supernormals and their average-ager counterparts over 2 years. ALFF measures the amplitude of low-frequency oscillations (0.01–0.08 Hz) induced by neuronal activity (Fox and Raichle 2007; Balduzzi et al. 2008; Zuo et al. 2010). Emerging evidence suggests ALFF may reflect neural synchronization across discrete brain regions (Buzsaki and Draguhn 2004; Balduzzi et al. 2008). Different from functional connectivity analysis which often requires pre-defined seeds or specific regions of interest, ALFF measure enables whole-brain voxel-wise analysis to identify distributed voxels that are related to successful cognitive aging. Meanwhile, altered ALFF has been observed in regions involved in the default mode network (Zang et al. 2007) as well as group with amnestic mild cognitive impairment (aMCI), a symptomatic preclinical stage of Alzheimer's disease (AD) (Ren et al. 2016). Altogether, ALFF may inform cognitive aging-related neural functional changes that are distributed in the brain and may be particularly suitable to differentiate the anterior versus posterior regions hypothesis tested here. Secondly, we internally validated the predictive value of the "Supernormal map" for cognitive function in the same set of older adults without cognitive impairment from the first step. Lastly, we validated the predictive value of the "Supernormal map" for AD pathophysiology in a separate set of older adults with and without AD. Here we were particularly interested in AD pathophysiology because AD is the most common aging-associated neurodegenerative disease, while AD pathophysiology is known to occur decades earlier than the onset of AD (Hardy and Selkoe 2002; Jack et al. 2010b; Jansen et al. 2015). Validating the "Supernormal map" for AD pathophysiology in older adults with a wide cognitive spectrum will facilitate the generalizability of the identified map in its clinical utility.

Materials and Methods

Data Source

Data used in this study were obtained from the ADNI database (adni.loni.usc.edu). The ADNI was launched in 2003 as a public-private partnership, led by Principal Investigator Michael W. Weiner, MD. The primary goal of ADNI has been to test whether serial MRI, positron emission tomography, other biological markers, and clinical and neuropsychological assessment can be combined to measure the progression of aMCI and early AD. Imaging protocols and procedures were developed for control

of data quality and scan consistency. Phantoms and strategies were also finalized to ensure the consistent acquisition of high quality data at the different sites (Jack et al. 2010a). For up-to-date information, see www.adni-info.org.

Participants

All participants in this study were enrolled in ADNIGO and ADNI2 where rs-fMRI data were collected using 3 T scanners. We conducted 3 steps to develop and validate the "Supernormal map": identification of a "Supernormal map", internal validation, and examination in the context of AD.

For the first 2 steps, we identified a group of older adults without cognitive impairment (referred to as "Normative" afterwards) [$n = 29$, including 13 Supernormals (SN_I) and 16 average-ager controls (AC_I)] who had consecutive rs-fMRI data and cognitive assessments at 2 time points (1 year apart) from our previous dataset (including 354 older adults free of dementia/mild cognitive impairment or major psychiatric disorders over the course of participating in ADNIGO and ADNI2) (Lin et al. 2017b). In previous analysis, we applied finite mixture models to examine 5-year trajectories of episodic memory (EM) and executive function (EF) standardized composite scores. The composite EM index was based on the memory-related learning and delayed domains of multiple memory tests (e.g., Rey Auditory Verbal Learning Test, Logical Memory test, etc.). The composite EF index was based on the Clock Draw Test, Category Fluency, and Trails A and B. The EF tests cover cognitive domains of visuospatial function, fluency, attention, and processing speed, which are all important for understanding aging or AD associated cognitive decline (Faust and Balota 1997; Shulman 2000). In ADNI dataset, EM and EF > 0 indicated intact cognitive performance; and the 2 composite indices have been validated to differentiate participants with or without AD, and to predict AD progression (Crane et al. 2012; Gibbons et al. 2012). Three latent classes were generated: "Successful agers" exhibited high and stable EM [Intercept (SE) = 1.51 (0.06); Slope (SE) = 0.003 (0.02)] and EF [Intercept (SE) = 1.05 (0.08); Slope (SE) = 0.08 (0.02)] over time; the other 2 classes exhibited high but gradually declined EM [Intercept (SE) = 1.41 (0.08); Slope (SE) = −0.05(0.02)] and EF [Intercept (SE) = 1.25 (0.08); Slope (SE) = −0.14 (0.02)] or low but intact EM [Intercept (SE) = 1.08 (0.20); Slope (SE) = −0.12 (0.07)] and EF [Intercept (SE) = 0.40 (0.07); Slope (SE) = −0.06 (0.02)] over time. "Successful agers" had significantly different intercept and slope in EM, as well as different slope in EF, from the other 2 classes. SN_I were selected from the "successful agers" while AC_I were from the other 2 classes. Of note, the latter 2 classes' performance remained normal (EM and EF > 0) over the course despite the slight decline, and a secondary analysis was conducted related to the class difference in the "Supernormal map" (see Results and Supplemental Fig. 1). In addition, there is no current consensus definition for successful cognitive aging. In our operationalization of the construct we consider successful cognitive aging to be longitudinally stable superior performance in multiple cognitive domains relative to age- and education-matched peers. In the present study, SN_I and AC_I significantly differed in EM at both time points, and differed in EF at follow-up (see Table 1).

For the last step, we identified a different group of 18 normative participants who only had rs-fMRI data at 1 time point as well as beta-amyloid and tau data from the previous dataset [including 6 Supernormals (SN_E) and 12 average-ager controls (AC_E)] (Lin et al. 2017b). We also identified stable aMCI (a group at high risk for AD, $n = 57$), as well as AD subjects ($n = 26$) from ADNI dataset who had 1 time point rs-fMRI data and beta-amyloid and tau data from the same 6-month window. The diagnoses of aMCI and AD were made by a psychiatrist or neurologist at each study site and reviewed by a Central Review Committee based on serial neuropsychological tests (details in Fig. 1). The 3 groups ($SN_E + AC_E$, aMCI, and AD) significantly differed in their cognitive performance (see Table 1).

Of note, all participants included in the present study were required to have rs-fMRI data collection within a 6-month window of the cognitive assessments. Other inclusion/exclusion criteria are described in Figure 1. The sample characteristics for the 2 datasets are presented in Table 1.

Identification of "Supernormal Map"

Data acquisition, preprocessing, and whole-brain searchlight analysis were conducted to determine the longitudinal neural profile of Supernormals using the dataset of 29 Normative (13 SN_I and 16 AC_I).

Data Acquisition and Preprocessing

All rs-fMRI data were collected using a 3.0 Tesla Phillips MRI with an echo-planar imaging sequence (TR = 3000 ms, TE = 30 ms, slice thickness = 3.3 mm, matrix = 64 × 64, spatial resolution = 3 × 3 × 3 mm^3, number of volumes = 140, number of slices = 48). Structural images were obtained using an MPRAGE sequence (TR/TE = 6.77/3.13 ms, TI = 0 ms, FA = 9°, matrix = 256 × 256, resolution 1 × 1 × 1 mm^3, slice thickness = 1 mm), which were then used for registration during preprocessing.

Across individuals, the first 10 volumes were discarded to avoid potential noise related to the equilibrium of the scanner and participant's adaptation process. The remaining 130 volumes were preprocessed using slice time correction and head motion correction. The images were then registered to each individual's own structural image, normalized to the Montreal Neurological Institute (MNI) standard space and spatially smoothed using a Gaussian kernel (FWHM = 4 mm). All preprocessing was conducted using the Data Processing Assistant for rs-fMRI package (Chao-Gan and Yu-Feng 2010).

ALFF Calculation

We followed the processing reported earlier (He et al. 2007; Ren et al. 2016). Briefly, after removing the linear trend, the time series of BOLD signals were converted to the frequency domain using the fast Fourier transform. ALFF value of each voxel was defined as the averaged square root of the power spectrum across 0.01–0.08 Hz using the Resting-State fMRI Data Analysis Toolkit (Song et al. 2011).

Voxel-based Morphometry Analysis

Since ALFF measurement was derived from gray matter (GM) (Zuo et al. 2010), here we extracted GM volume to control for potential brain atrophy in the following analysis. Voxel-based morphometry (VBM) was performed using the SPM8 package (http://www.fil.ion.ucl.ac.uk/spm). Briefly, the structural images were segmented into GM, white matter, and cerebrospinal fluid. After an initial affine registration of the GM map into the MNI space, the GM images were nonlinearly warped using diffeomorphic anatomical registration through Exponentiated Lie Algebra (Ashburner 2007).

Whole-brain Searchlight Analysis

We used searchlight analysis, a multivariate method with whole-brain ALFF data to identify voxels that discriminate SN_I

Table 1. Sample characteristics

Identification of "Supernormal map" and internal validation		SN_I ($N = 13$)	AC_I ($N = 16$)	T, F, or χ^2 test, df (P)
Age baseline, Mean (SD)		76.46 (7.52)	75.19 (6.62)	0.49, 27 (0.63)
Male, *N* (%)		5 (38.5)	8 (50)	0.39, 1 (0.53)
Education, Mean (SD)		16.23 (2.24)	16.13 (2.5)	0.12, 27 (0.91)
APOE4 carrier, *N* (%)		4 (30.8)	6 (37.5)	0.14, 1 (0.71)
GM volume baseline, Mean (SD)		0.36 (0.04)	0.36 (0.04)	−0.38, 27 (0.71)
GM volume follow-up, Mean (SD)		0.36 (0.04)	0.36 (0.04)	−0.20, 27 (0.84)
EM baseline, Mean (SD)		1.35 (0.37)	0.89 (0.58)	**2.45, 27 (0.021)**
EM follow-up, Mean (SD)		1.34 (0.39)	0.91 (0.47)	**2.63, 27 (0.014)**
EF baseline, Mean (SD)		1.11 (0.52)	0.73 (0.71)	1.59, 27 (0.12)
EF follow-up, Mean (SD)		1.28 (0.54)	0.51 (0.36)	**3.19, 27 (0.004)**
MOCA baseline, Mean (SD)		26.85 (1.77)	25 (2.03)	**2.57, 27 (0.016)**
MOCA follow-up, Mean (SD)		27 (2.35)	25.25 (2.52)	1.92, 27 (0.066)
External validation	$SN_E + AC_E$ ($N = 18$)	aMCI ($N = 57$)	AD ($N = 26$)	χ^2 or F-test, df1, df2 (P)
Age, Mean (SD)	71.78 (6.28)	71.95 (7.89)	73.75 (7.35)	0.59, 2, 98 (0.56)
Male, *N* (%)	9 (50)	31 (54.39)	13 (50)	0.19, 2 (0.91)
Education, Mean (SD)	17.56 (1.98)[a]	16.18 (2.63)[b]	15.38 (2.67)[b]	**3.91, 2, 98 (0.023)**
APOE4 carrier, *N* (%)	7 (38.9)[a]	25 (43.9)[a]	20 (76.9)[b]	**9.21, 2 (0.010)**
GM volume, Mean (SD)	0.34 (0.03)	0.33 (0.03)	0.32 (0.04)	1.90, 2, 98 (0.16)
Aβ/pTau ratio, Mean (SD)	6.18 (3.40)[a]	5.97 (4.24)[a]	3.27 (2.19)[b]	**5.44, 2, 98 (0.006)**
EM, Mean (SD)	1.20 (0.58)[a]	0.29 (0.70)[b]	−1.01 (0.63)[c]	**7.96, 2, 92 (0.001)**
EF, Mean (SD)	0.83 (0.61)[a]	0.38 (0.86)[a]	−1.03 (0.83)[c]	**8.56, 2, 92 (<0.001)**
MOCA, Mean (SD)	26.22 (2.70)[a]	23.30 (6.03)[b]	16.10 (8.04)[c]	**43.05, 2, 90 (<0.001)**

SN_I, Supernormals; AC_I, average-ager controls (for *Identification of "Supernormal map"* and *Internal validation*); SN_E, Supernormals; AC_E, average-ager controls (for *Examination in the context of AD*); aMCI, amnestic mild cognitive impairment; AD, Alzheimer's disease; APOE4, apolipoprotein E ε4; SD, standard deviation; GM, gray matter; Aβ, Beta-amyloid-(1-42); EM, episodic memory; EF, executive function; MOCA, Montreal Cognitive Assessment.
Note. [a, b, c] represents the post-hoc comparison difference from the *F*-test. Bold values indicate $P < 0.05$.

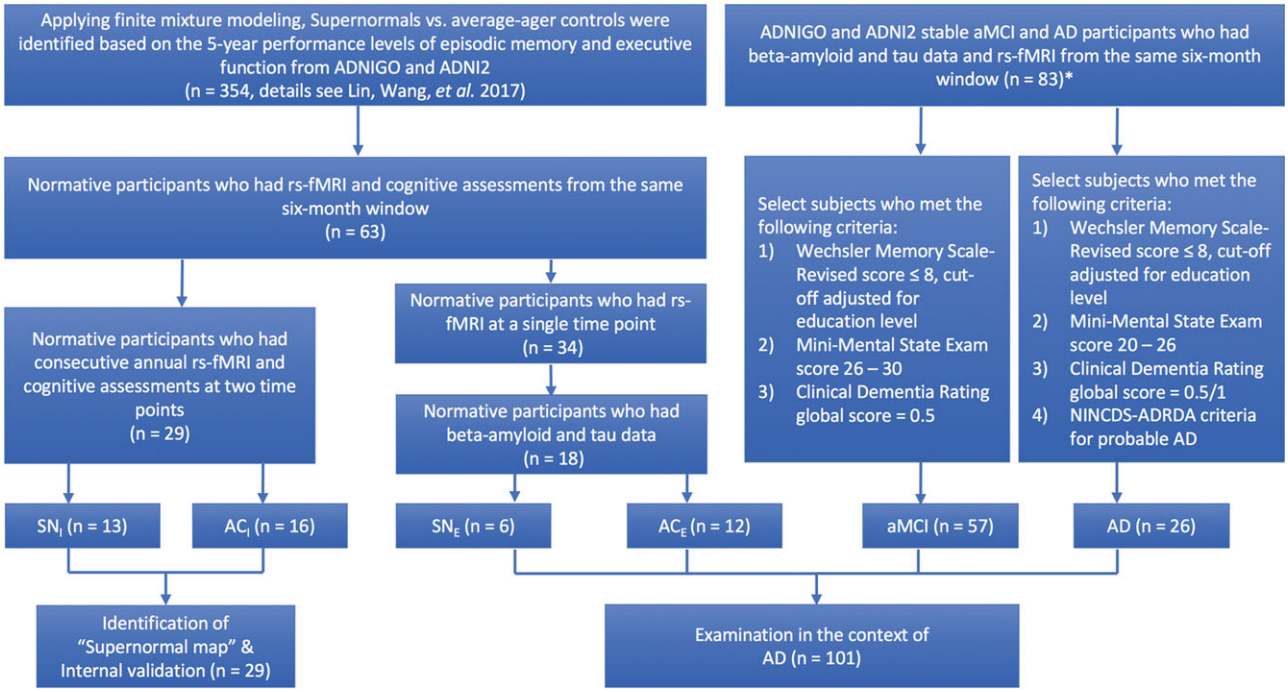

Figure 1. Sample selection flow chart. Note. rs-fMRI, resting-state functional magnetic resonance imaging; aMCI, amnestic mild cognitive impairment; AD, Alzheimer's disease; SN_I, Supernormals; AC_I, average-ager controls (for *Identification of "Supernormal map"* and *Internal validation*); SN_E, Supernormals; AC_E, average-ager controls (for *Examination in the context of AD*). *If the participants had more than one time points' data, a random selection that corresponded to the beta-amyloid and pTau data was used.

and AC_I at baseline and follow-up separately. Compared to univariate approaches where each brain region or cluster that can differentiate 2 groups is analyzed separately, multivariate approaches focus on discovering multiple functionally relevant voxels that have discriminative power from distributed locations simultaneously (Uddin et al. 2011). Searchlight analysis measures signals present in small voxel subsets, providing increased sensitivity and flexibility in identifying neural clusters or patterns that are distributed across multiple neurons or regions at the whole-brain scale (Kriegeskorte et al. 2006; Etzel et al. 2013). Briefly, for a given voxel (Vi), its searchlight was defined as a cube with an edge length of 3 voxels centered at Vi ($3 \times 3 \times 3$ dimensional). Within this searchlight, the spatial pattern was defined by a 27-dimensional vector. We extracted the spatial pattern from the ALFF data within the searchlight for the subjects ($N = 29$) and then performed leave-one-out-cross-validation (LOOCV) (Pereira et al. 2009) classification using the Gaussian Naïve Bayes classifier (Mitchell et al. 2004). The percentage of correct classifications was then noted at the center voxel Vi as the local classification information for the searchlight. The process was then conducted for all brain voxels, yielding a 3-dimensional map of cross-validation accuracy at every voxel ("searchlight map").

Statistical significance was calculated using permutation tests (Nichols and Holmes 2002). First, we randomly permuted the group labels for the subjects. We then performed searchlight analysis on whole-brain ALFF data using permuted class labels (the processing and cross-validation schemes were identical to the process with true group labels). The permutation test was then repeated 50 000 times, resulting in a distribution of permutation accuracy for each searchlight. We counted the number of times where the permutation accuracy was greater than the accuracy obtained based on true class labels. Each searchlight's P-value was reported as (number of permutation accuracy > true accuracy)/number of permutations.

"Supernormal Map" Identification

From the searchlight maps, we first identified voxels with high classification accuracies (classification accuracy > 65%, FDR corrected $P < 0.05$, cluster size > 20 voxels) at baseline ("map at baseline", 5060 voxels; Fig. 2, blue voxels) and follow-up ("map at follow-up", 12 740 voxels; Fig. 2, yellow voxels) separately. The "Supernormal map" was defined as the overlap in preserved regions (voxels that were retained in both "map at baseline" and "map at follow-up"), meaning that the "Supernormal map" corresponds to regions that consistently show high discriminative power between SN_I and AC_I across time (1642 voxels, Fig. 2, green voxels). For descriptive purposes, we also calculated the mean searchlight accuracy between SN_I and AC_I across time within the "Supernormal map". To compare the level of brain oscillations within the "Supernormal map" between SN_I and AC_I, we extracted ALFF values within the map from SN_I and AC_I at baseline and follow-up, respectively. Two-sample t-tests were applied to quantify the difference of oscillations between groups at each time (Fig. 3).

For comparison, we also extracted the "discrepancy map", defined as voxels that were unique in the "map at follow-up" but not in the "map at baseline" (10 879 voxels, Fig. 2, copper voxels). Of note, the discrepancy between SN and AC widened with aging, resulting in more voxels with discriminative capacity in follow-up.

To understand the brain structure, we extracted GM volumes within the "Supernormal map" as well as within the whole brain. We then performed a repeated-measure ANOVA to estimate time (baseline vs. follow-up) by group (SN_I vs. AC_I) effects on GM volumes. P-value was set at <0.05 for the analysis.

Internal Validation

The goal of internal validation was to validate the predictive power of the "Supernormal map" on "global cognition", which was measured using the Montreal Cognitive Assessment (MOCA) (Rossetti et al. 2011), a commonly used cognitive screening test comprised of subtests measuring executive, visuospatial, memory, language, and attention abilities. For the MOCA, we acquired data at baseline, follow-up, and longitudinal change (follow-up—baseline). We converted the total MOCA scores to z-scores and used them for the following regression analyses. In addition, we performed repeated-measure ANOVA to estimate time (baseline vs. follow-up) by group (SN_I vs. AC_I) effects on the MOCA. Of note, we used MOCA for the internal validation process since it was not part of the characterization for Supernormals, and MOCA covers multiple cognitive domains than EM/EF (Rossetti et al. 2011) (in our previous study, only 16–25% of the variance in EM and EF was explained by MOCA (Lin et al. 2017b).

Regression on MOCA using the "Supernormal map": To ensure the validity of the results, we examined change in MOCA over time using 2 analytical strategies: 1) taking MOCA at follow-up as the outcome controlling for baseline measure, and 2) taking the longitudinal change (follow-up—baseline) in MOCA as the outcome. For model (1), age (at follow-up), sex, APOE4, and the GM volume (at follow-up) were included as covariates, while ALFF features (ALFF values of voxels) from the "Supernormal map" at baseline were the predictor. For model (2), age (at baseline), sex, APOE4, and the change of GM volume were included as covariates while longitudinal change (follow-up—baseline) of ALFF features from the "Supernormal map" were the predictor.

As a comparison, we used ALFF features from the "map at baseline", "map at follow-up", and "discrepancy map", respectively, and repeated the regression using the 2 types of analytical strategies. Same sets of covariates were applied.

During regression, ALFF features were scaled to [−1, 1] to ensure similarity of ranges for feature values and comparable contribution of each feature to the final regression from both training and test sets (Chang and Lin 2011). We retained the LOOCV partition scheme and used epsilon-insensitive support vector regression (ε-SVR) (Dosenbach et al. 2010) with the linear kernel (Hsu et al. 2003) to predict changes of MOCA. For ε-SVR, all identified voxels' ALFF values were used as candidate predictors. The support vectors (i.e., final predictors selected from candidate predictors) and the penalty parameter C jointly controlled the final regression line. The process was in essence performing linear regression in hyperspace using ε-insensitive loss: an epsilon-tube around the regression line in hyperspace was defined, no penalty was assigned for any training data within the tube; whereas data beyond the tube were penalized. The parameters (penalty parameter C, tolerance ε) of the ε-SVR model were selected using a grid search on subsets of the data and then fed into the final regression models. After regression, we evaluated the results by performing model fitting of the observed and predicted cognitive measurements using the linear function $y = ax + b$. Adjusted R^2 was used to estimate goodness of fit for the model. The regression was implemented using LIBSVM library (Chang and Lin 2011). All statistical testing and curve fitting were conducted using MATLAB R2015a (The Mathworks, Natick, MA).

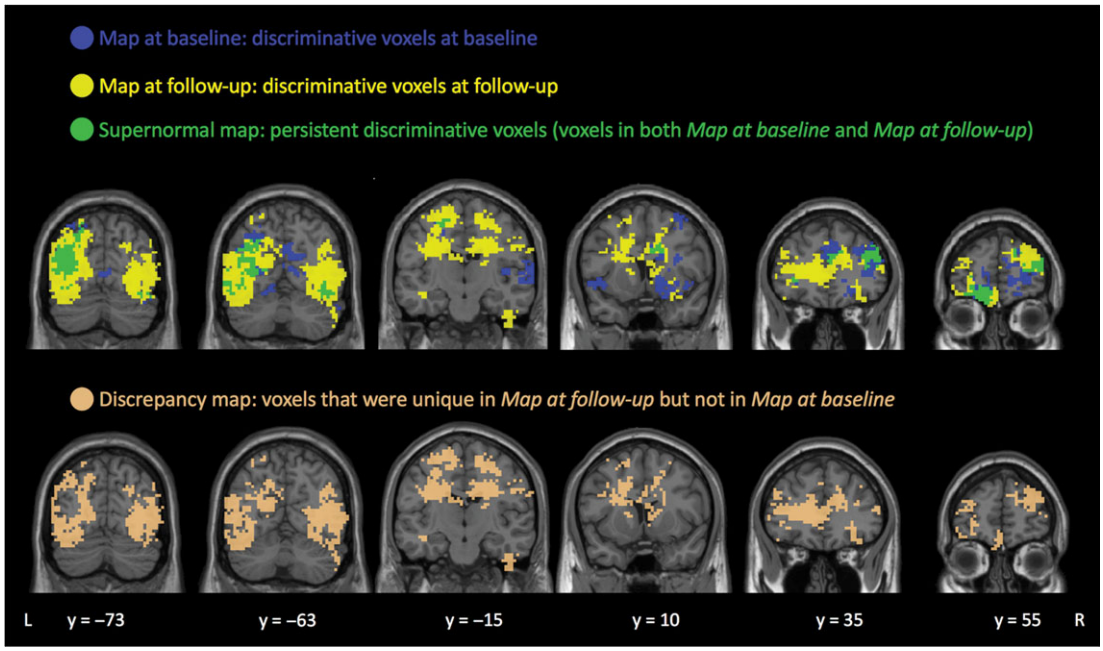

Figure 2. Identified voxels from searchlight classification of Supernormals and average-ager controls. "Supernormal map" (green) includes voxels that were retained in both "map at baseline" (blue) and "map at follow-up" (yellow). "Discrepancy map" (copper) includes voxels that were unique in the "map at follow-up" but not the "map at baseline". *Note*. L, left; R, right.

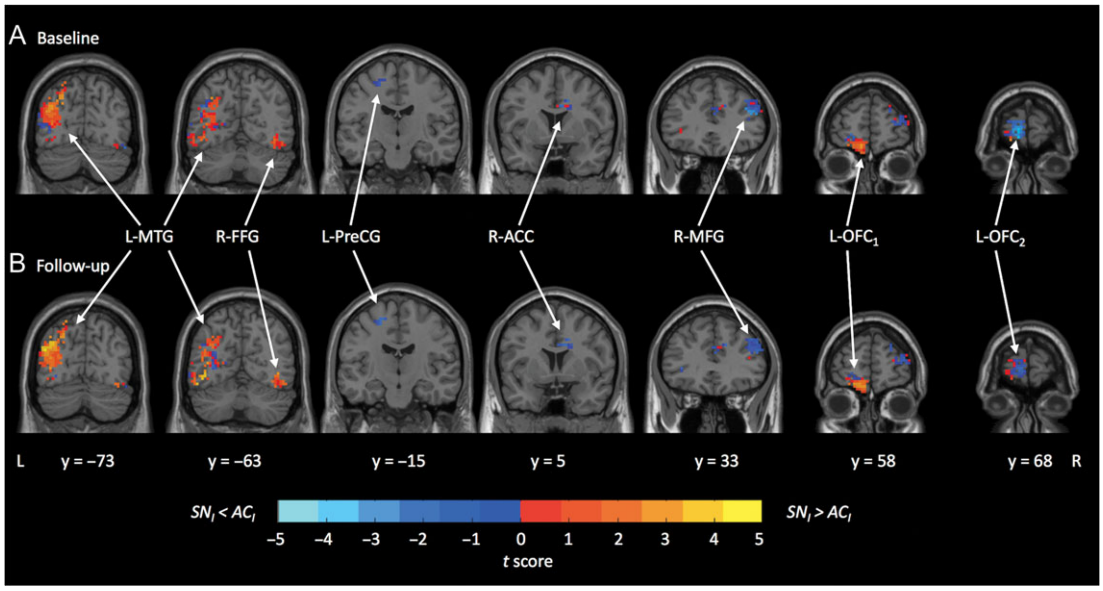

Figure 3. Regional oscillation difference between SN_I and AC_I within the "Supernormal map". (A) Oscillation difference at baseline. (B) Oscillation difference at follow-up. *Note*. The color bar indicates the scale for the *t*-statistic. Hot/cold colors indicate stronger/weaker oscillations in SN_I compared to AC_I. L-MTG, left middle temporal gyrus; R-FFG, right fusiform gyrus; L-PreCG, left precentral gyrus; R-ACC, right anterior cingulate cortex; R-MFG, right middle frontal gyrus; L-OFC, left orbitofrontal cortex; SN, Supernormals; AC, average-ager controls; L, left; R, right. Figures were generated using Data Processing & Analysis for Brain Imaging toolbox (Yan et al. 2016).

Examination in the Context of AD

This step aimed to examine relationships between the "Supernormal map" and AD pathology. Here we extracted ALFF features of the "Supernormal map" from a separate dataset [18 Normative (6 SN_E and 12 AC_E), 57 aMCI and 26 AD]. We used the identified map to predict AD pathology.

AD pathology: Beta-amyloid-(1–42) (Aβ) and pTau were derived from cerebrospinal fluid aliquots and measured using the multiplex xMAP Luminex platform (Luminex Corp., Austin, Tex., USA) with immunoassay kit-based reagents (INNO-BIA AlzBio3; Innogenetics, Ghent, Belgium). Aβ and pTau data used in the present study were from the same time point as the rs-fMRI data for the independent sample. The Aβ/pTau ratio was used as the "AD signature" for which lower Aβ/pTau ratio indicated an increased burden of AD pathology (De Meyer et al. 2010).

AD pathology regression: We converted the Aβ/pTau ratios to z-scores and used ε-SVR with a linear kernel to predict them

Table 2. Regions consistently showed high discriminative power between Supernormals and average-ager controls across time in the "Supernormal map"

	Region	Size of cluster (voxels)	Peak mean classification accuracy across time	t-value	P-value	Peak MNI coordinates		
						x	y	z
Oscillations of $SN_I > AC_I$	L-MTG	125	0.87	4.20	<0.001	−45	−75	15
	$L\text{-}OFC_1$	88	0.75	3.84	0.01	−18	60	−18
	R-FFG	16	0.79	3.03	<0.001	42	−63	−15
Oscillations of $SN_I < AC_I$	L-PreCG	30	0.77	3.15	<0.001	−24	−15	54
	$L\text{-}OFC_2$	33	0.70	4.06	0.02	−9	69	0
	R-ACC	27	0.79	2.76	0.02	18	3	33
	R-MFG	208	0.85	3.16	<0.001	45	24	33

Note. All results are thresholded at $P < 0.05$ (FDR corrected). MNI, Montreal Neurological Institute; SN, Supernormals; AC, average-ager controls; L-MTG, left middle temporal gyrus; L-OFC, left orbitofrontal cortex; R-FFG, right fusiform gyrus; L-PreCG, left precentral gyrus; R-ACC, right anterior cingulate cortex; R-MFG, right middle frontal gyrus.

from the "Supernormal map". Age, sex, years of education, APOE, and GM volume were added as covariates. Years of education was controlled here due to the group difference in this variable (see Table 1). Other details of the regression analysis are as described in section "Internal Validation".

Results

Identified "Supernormal Map"

The "Supernormal map" consists of the right fusiform gyrus (R-FFG), right middle frontal gyrus (R-MFG), right anterior cingulate cortex (R-ACC), left middle temporal gyrus (L-MTG), left precentral gyrus (L-PreCG), and left orbitofrontal cortex (L-OFC). These regions showed mean classification accuracy ranging from 0.70 to 0.87 between SN_I and AC_I across time (Table 2).

Within the "Supernormal map", we found higher oscillations in the L-MTG, R-FFG, while lower oscillations in the L-PreCG, R-ACC, and R-MFG in SN_I compared to AC_I at both baseline and follow-up. Mixed patterns of oscillations were found in the L-OFC (higher oscillations in $L\text{-}OFC_1$, lower oscillations in $L\text{-}OFC_2$ in SN_I compared to AC_I at both time points) (Fig. 3). For a secondary analysis, we compared the oscillations within the "Supernormal map" between 2 classes of average-agers involved in AC_I reported in our previous paper (Lin et al. 2017b). We did not find any distinct difference in the oscillations between the 2 classes, suggesting the functional similarity in the 2 average-ager classes (Supplementary Fig. 1).

A repeated-measure ANOVA for GM volume within the "Supernormal map" or the whole brain showed no significant time (baseline vs. follow-up) or group (SN_I vs. AC_I) main effects or interaction effect (all $P > 0.05$).

Internal Validation

SN_I and AC_I significantly differed in MOCA at baseline (see Table 1). A repeated-measure ANOVA for MOCA showed a significant group (SN_I vs. AC_I) main effect ($F_{1,27} = 6.04$, $P = 0.021$) but no time by group interaction effect.

Using ε-SVR (controlling for relevant covariates), ALFF features extracted using the "Supernormal map" strongly predicted MOCA. "MOCA at follow-up controlling for MOCA at baseline": adjusted $R^2 = 0.68$ ($P < 0.001$); and "longitudinal changes of MOCA": adjust $R^2 = 0.62$ ($P < 0.001$) (Fig. 4A).

As comparisons, the ε-SVR on MOCA changes using ALFF features from the "map at baseline", "map at follow-up", and "discrepancy map" provided prediction results of adjusted R^2 ranged 0.02–0.20 (P ranged 0.06 to 0.72) (Fig. 4B,D).

Examination in the Context of AD

Controlling for covariates, ε-SVR on Aβ/pTau ratio using ALFF features extracted from "Supernormal map" reached adjusted $R^2 = 0.66$ ($P < 0.001$) (Fig. 5).

Discussion

Here we identify a "Supernormal map"—a set of brain regions whose longitudinal stability in their low-frequency oscillations—characterizing a state of successful cognitive aging. The "Supernormal map" includes the R-FFG, R-MFG, R-ACC, L-MTG, L-PreCG, and L-OFC (Fig. 2, green voxels, Fig. 3). The map strongly predicts 1 year change in global cognition (measured using MOCA, adjusted R^2 ranged 0.62–0.68, Fig. 4), and was also strongly correlated to Alzheimer's pathology (mean adjusted $R^2 = 0.66$, Fig. 5). We confirmed the hypothesis that some specific brain regions, the functional level of which, either active or deactive, remaining relatively stable over time, contributed to the explanation of the Supernormal phenomenon (Lindenberger 2014).

Compared to average-ager controls, Supernormals tend to have consistently higher oscillations in the L-MTG, R-FFG and $L\text{-}OFC_1$, and lower oscillations in the L-PreCG, R-ACC, R-MFG, and $L\text{-}OFC_2$ across time points. The location and direction of oscillations in most of the regions are consistent with previous investigation of neural mechanisms, especially high neural reserve while low neural compensation (Stern et al. 2008). For example, maintaining high activation of the medial temporal lobe was related to slower decline in memory performance in healthy older adults (Persson et al. 2012), which is consistent with our findings in the MTG for Supernormals. Also, active FFG in memory tasks was observed in both younger adults, relative to older adults (Gutchess et al. 2005), and cognitively healthy older adults, relative to patients with AD (Scarmeas et al. 2004). On the other hand, increased activation in the MFG, PreCG, or ACC during various cognitive tasks was often observed in older adults compared to younger adults, compensating for the decreased neural efficiency in posterior brain regions (Gutchess et al. 2005; Waiter et al. 2008; Hampshire et al. 2010). Noticeably, the oscillation patterns among Supernormals in the present study are more alike those reported by younger adults in the literature, further supporting their reserved neural capacity. Reliance on neural reserve to

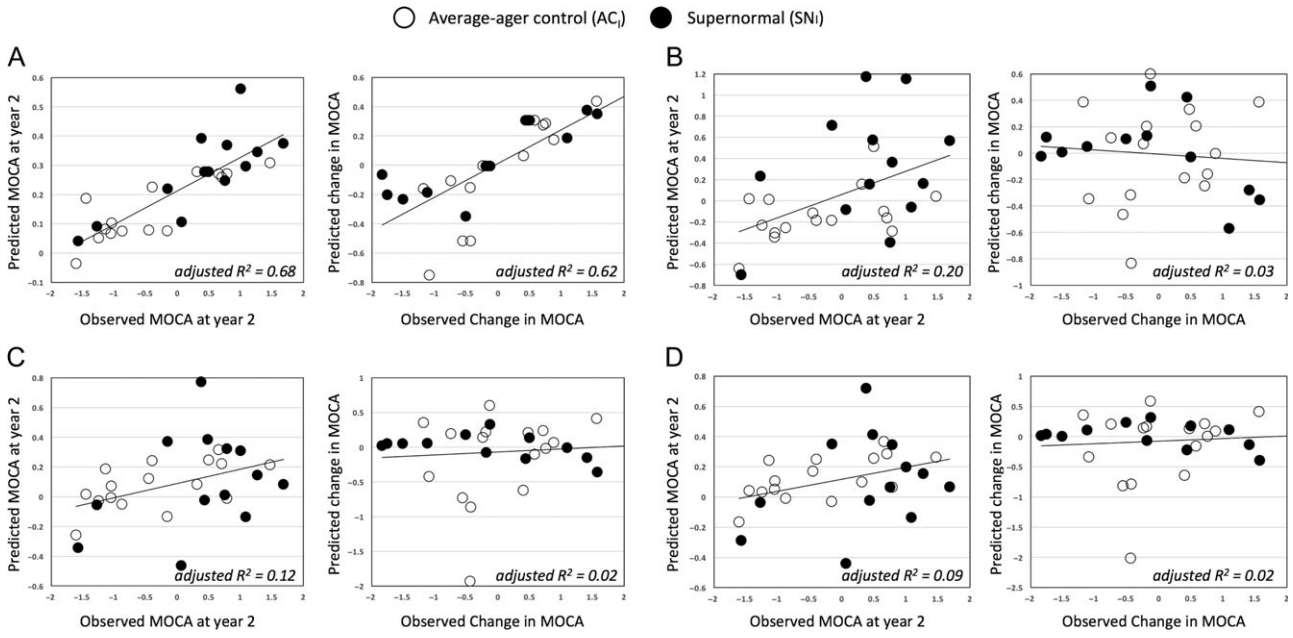

Figure 4. Regression on MOCA using ALFF features from different maps in SN$_I$ and AC$_I$. Regression on MOCA at follow-up adjusting for relevant baseline measure (left); regression on longitudinal change (follow-up year 1) of MOCA (right) using ALFF features from the "Supernormal mask" (*A*), "map at baseline" (*B*), "map at follow-up" (*C*), and "discrepancy mask" (*D*). In all models, age, sex, APOE4, and GM volume were controlled. *Note.* Jitter-observed MOCA values were used to avoid overplotting.

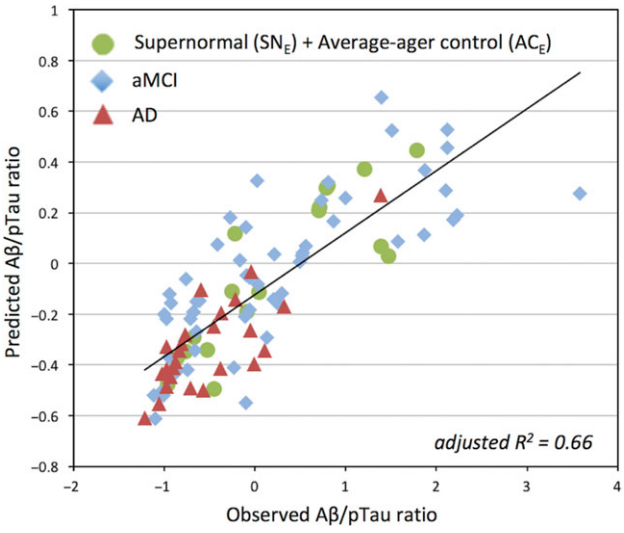

Figure 5. Regression on Aβ/pTau ratio using ALFF features from the "Supernormal map". Age, sex, years of education, APOE, and GM volume were controlled. *Note.* Jitter-observed Aβ/pTau values were used to avoid overplotting.

maintain cognitive function is a signature of younger and healthier brain (Stern 2002). However, we should acknowledge that the "Supernormal map" does not completely meet another criterion for "youth brain" related to lateralization. Previous studies observed greater right hemisphere involvement for executive function and memory tasks in younger age (Kelley et al. 1998; Carpenter et al. 2000). Meanwhile, age-related cognitive decline affects the functional attributions in the right hemisphere to a greater degree than those in the left hemisphere (Goldstein and Shelly 1981; Grady et al. 1994; Jockwitz et al. 2017). In the present study, Supernormals seem to rely on both hemispheres. This phenomenon may relate to the "successful compensation" discussed previously that supports successful cognitive aging (Lindenberger 2014). Lastly, similar to previous studies of mixed relationship between the OFC's volume and cognitive performance in aging (Salat et al. 2002; Zimmerman et al. 2006), the exact functional role of OFC in Supernormals is yet to be determined.

Furthermore, we linked the "Supernormal map" with the context of AD. Noticeably, most regions in the map are part of the default mode network (e.g., R-ACC, R-MFG, and L-PreCG) or executive control network (e.g., L-MTG), which are compromised in AD-related neurodegeneration (Sorg et al. 2007). The strong relationship between the "Supernormal map" and AD pathology may suggest that the adaptive plasticity (e.g., biochemical integrity; Mapstone et al. 2016) among Supernormals compensates for or resists the neurodegeneration-related changes, which may help protect against the pathological deposition within and outside these default networks. However, to better understand the relationship between AD pathology and the "Supernormal map", future studies will be required to investigate the exact AD pathology within the "Supernormal map". Also, with a larger sample size in Supernormals in the future, we will need to investigate the predictive value of the "Supernormal map" in classifying the phenotypes across the cognitive aging spectrum from Supernormal, average-agers, aMCI, to AD.

We need to acknowledge that the sample size for generating the "Supernormal map" was small (SN$_I$ = 13, AC$_I$ = 16), and we only utilized data from 2 time points. Here we used the stability of cross-time data derived from the searchlight analysis to identify the "Supernormal map" while there are other ways of comparing group difference in longitudinal imaging data in which a participant can be their own control (e.g., repeated measures of ANOVA). Besides, we should recognize that performing searchlight analysis requires to minimize the spatial misalignment across participants. Although we preprocessed

and registered all participants' data to the MNI template, there may still be inter-subject alignment mismatch. There may also be limitation related to the use of the ADNI dataset in both "Supernormal map" identification and the examination related to AD (even though we used 2 different sets of sample), which needs to be further validated in other datasets, including the work related to the AD phenotype classification. Also, the ADNI dataset includes only adults aged 55–90 years, future studies involving the comparison of Supernormals' brain functions with young or middle-age adults are needed. Next, previous studies have identified unique subgroups of older adults that demonstrated strong cognitive ability and investigated the relevant anatomic, genetic, and behavioral factors (Waiter et al. 2008; Rogalski et al. 2013; Sun et al. 2016; Bott et al. 2017). To further characterize the Supernormal group identified in our study, other biological and lifestyle factors and their relationships with the "Supernormal map" needs to be tested. Furthermore, there is a lack of consensus on how to define successful cognitive aging. Here we incorporated 5-year superior performance of multiple cognitive domains (episodic memory and executive function) as exemplars of successful aging (Lin et al. 2017b), but we acknowledge that other studies need to be conducted to further prove the validity of the "Supernormal map". Finally, unlike previous work where lesser decline of cortical thickness was observed in Supernormals (Cook et al. 2017), GM volumes within the "Supernormal map" or the whole brain were not significantly different between groups in our study. We suspected such discrepancy may result from the difference in the age ranges between studies (i.e., ours were 10 years younger than Cook et al.'s). Along with other concerns on the lack of younger comparison, it is necessary to validate the "Supernormal map" in a wider age range.

In summary, by constructing a functional brain map with longitudinally stable oscillations for older adults with exceptional cognitive performance, we confirmed that some brain regions whose function have the potential to be resistant to the effects of aging or aging-associated neurodegeneration. The regions, especially the differential levels of oscillations between anterior and posterior parts, involved in the "Supernormal map" may provide the biomarkers for future work on promoting successful cognitive aging and preventing cognitive decline.

Supplementary Material

Supplementary data are available at *Cerebral Cortex* online.

Funding

This work was supported by the National Institutes of Health (grant number NR015452, AG053193), as well as University of Rochester Goergen Institute for Data Science Collaborative Pilot Aware Program in Health Analytics and Furth Fund to F. Lin.

Data used in the preparation of this article were obtained from the Alzheimer's Disease Neuroimaging Initiative (ADNI). Data collection and sharing of ADNI were funded by the National Institutes of Health Grant U01 AG024904 and Department of Defense award number W81XWH-12-2-0012. ADNI is funded by the National Institute on Aging, the National Institute of Biomedical Imaging and Bioengineering, and through generous contributions from the following: Alzheimer's Association; Alzheimer's Drug Discovery Foundation; BioClinica, Inc.; Biogen Idec Inc.; Bristol-Myers Squibb Company; Eisai Inc.; Elan Pharmaceuticals, Inc.; Eli Lilly and Company; F. Hoffmann-La Roche Ltd and its affiliated company Genentech, Inc.; GE Healthcare; Innogenetics, N.V.; IXICO Ltd.; Janssen Alzheimer Immunotherapy Research & Development, LLC.; Johnson & Johnson Pharmaceutical Research & Development LLC.; Medpace, Inc.; Merck & Co., Inc.; Meso Scale Diagnostics, LLC.; NeuroRx Research; Novartis Pharmaceuticals Corporation; Pfizer Inc.; Piramal Imaging; Servier; Synarc Inc.; and Takeda Pharmaceutical Company. The Canadian Institutes of Health Research is providing funds to support ADNI clinical sites in Canada. Private sector contributions are facilitated by the Foundation for the National Institutes of Health (www.fnih. org). The grantee organization is the Northern California Institute for Research and Education, and the study is coordinated by the Alzheimer's Disease Cooperative Study at the University of California, San Diego. ADNI data are disseminated by the Laboratory for Neuro Imaging at the University of California, Los Angeles.

Notes

We thank Andrew J. Anderson, Julian Gal, Kelsey McDermott, Yuchuan Zhuang, and Jiayi Zhou for providing comments. *Conflict of Interest*: None declared.

References

Andrews-Hanna JR, Snyder AZ, Vincent JL, Lustig C, Head D, Raichle ME, Buckner RL. 2007. Disruption of large-scale brain systems in advanced aging. Neuron. 56:924–935.

Ashburner J. 2007. A fast diffeomorphic image registration algorithm. Neuroimage. 38:95–113.

Balduzzi D, Riedner BA, Tononi G. 2008. A BOLD window into brain waves. Proc Natl Acad Sci U S A. 105:15641–15642.

Baltes MM, Carstensen LL. 1996. The process of successful ageing. Ageing Soc. 16:397–422.

Bott NT, Bettcher BM, Yokoyama JS, Frazier DT, Wynn M, Karydas A, Yaffe K, Kramer JH. 2017. Youthful processing speed in older adults: genetic, biological, and behavioral predictors of cognitive processing speed trajectories in aging. Front Aging Neurosci. 9:55.

Burgmans S, van Boxtel MPJ, Vuurman EFPM, Smeets F, Gronenschild EHBM, Uylings HBM, Jolles J. 2009. The prevalence of cortical gray matter atrophy may be overestimated in the healthy aging brain. Neuropsychology. 23:541–550.

Buzsaki G, Draguhn A. 2004. Neuronal oscillations in cortical networks. Science. 304:1926–1929.

Carpenter PA, Just MA, Reichle ED. 2000. Working memory and executive function: evidence from neuroimaging. Curr Opin Neurobiol. 10:195–199.

Chang CC, Lin CJ. 2011. LIBSVM: a library for support vector machines. Acm Trans Intell Syst Technol. 2:27.

Chao-Gan Y, Yu-Feng Z. 2010. DPARSF: a MATLAB toolbox for "Pipeline" data analysis of resting-state fMRI. Front Syst Neurosci. 4:13.

Cook AH, Sridhar J, Ohm D, Rademaker A, Mesulam M-M, Weintraub S, Rogalski E. 2017. Rates of cortical atrophy in adults 80 years and older with superior vs average episodic memory. JAMA. 317:1373–1375.

Crane PK, Carle A, Gibbons LE, Insel P, Mackin RS, Gross A, Jones RN, Mukherjee S, Curtis SM, Harvey D, et al. 2012. Development and assessment of a composite score for memory in the Alzheimer's Disease Neuroimaging Initiative (ADNI). Brain Imaging Behav. 6:502–516.

De Meyer G, Shapiro F, Vanderstichele H, Vanmechelen E, Engelborghs S, De Deyn PP, Coart E, Hansson O, Minthon L, Zetterberg H, et al. 2010. Diagnosis-independent Alzheimer

disease biomarker signature in cognitively normal elderly people. Arch Neurol. 67:949–956.
Dosenbach NU, Nardos B, Cohen AL, Fair DA, Power JD, Church JA, Nelson SM, Wig GS, Vogel AC, Lessov-Schlaggar CN, et al. 2010. Prediction of individual brain maturity using fMRI. Science. 329:1358–1361.
Etzel JA, Zacks JM, Braver TS. 2013. Searchlight analysis: promise, pitfalls, and potential. Neuroimage. 78:261–269.
Faust ME, Balota DA. 1997. Inhibition of return and visuospatial attention in healthy older adults and individuals with dementia of the Alzheimer type. Neuropsychology. 11:13–29.
Fjell AM, Sneve MH, Storsve AB, Grydeland H, Yendiki A, Walhovd KB. 2016. Brain events underlying episodic memory changes in aging: a longitudinal investigation of structural and functional connectivity. Cereb Cortex. 26:1272–1286.
Fox MD, Raichle ME. 2007. Spontaneous fluctuations in brain activity observed with functional magnetic resonance imaging. Nat Rev Neurosci. 8:700–711.
Gefen T, Peterson M, Papastefan ST, Martersteck A, Whitney K, Rademaker A, Bigio EH, Weintraub S, Rogalski E, Mesulam MM, et al. 2015. Morphometric and histologic substrates of cingulate integrity in elders with exceptional memory capacity. J Neurosci. 35:1781–1791.
Gefen T, Shaw E, Whitney K, Martersteck A, Stratton J, Rademaker A, Weintraub S, Mesulam MM, Rogalski E. 2014. Longitudinal neuropsychological performance of cognitive superagers. J Am Geriatr Soc. 62:1598–1600.
Gibbons LE, Carle AC, Mackin RS, Harvey D, Mukherjee S, Insel P, Curtis SM, Mungas D, Crane PK, et al, Alzheimer's Disease. 2012. A composite score for executive functioning, validated in Alzheimer's Disease Neuroimaging Initiative (ADNI) participants with baseline mild cognitive impairment. Brain Imaging Behav. 6:517–527.
Goldstein G, Shelly C. 1981. Does the right hemisphere age more rapidly than the left? J Clin Neuropsychol. 3:65–78.
Grady CL, Maisog JM, Horwitz B, Ungerleider LG, Mentis MJ, Salerno JA, Pietrini P, Wagner E, Haxby JV. 1994. Age-related changes in cortical blood flow activation during visual processing of faces and location. J Neurosci. 14:1450–1462.
Gutchess A. 2014. Plasticity of the aging brain: new directions in cognitive neuroscience. Science. 346:579–582.
Gutchess AH, Welsh RC, Hedden T, Bangert A, Minear M, Liu LL, Park DC. 2005. Aging and the neural correlates of successful picture encoding: frontal activations compensate for decreased medial-temporal activity. J Cogn Neurosci. 17:84–96.
Hampshire A, Chamberlain SR, Monti MM, Duncan J, Owen AM. 2010. The role of the right inferior frontal gyrus: inhibition and attentional control. Neuroimage. 50:1313–1319.
Hardy J, Selkoe DJ. 2002. The amyloid hypothesis of Alzheimer's disease: progress and problems on the road to therapeutics. Science. 297:353–356.
Harrison TM, Weintraub S, Mesulam MM, Rogalski E. 2012. Superior memory and higher cortical volumes in unusually successful cognitive aging. J Int Neuropsychol Soc. 18:1081–1085.
He Y, Wang L, Zang Y, Tian L, Zhang X, Li K, Jiang T. 2007. Regional coherence changes in the early stages of Alzheimer's disease: a combined structural and resting-state functional MRI study. Neuroimage. 35:488–500.
Hsu C-W, Chang C-C, Lin C-J 2003. "A practical guide to support vector classification".
Jack CR Jr., Bernstein MA, Borowski BJ, Gunter JL, Fox NC, Thompson PM, Schuff N, Krueger G, Killiany RJ, Decarli CS, et al. 2010a. Update on the magnetic resonance imaging core of the Alzheimer's disease neuroimaging initiative. Alzheimers Dement. 6:212–220.
Jack CR Jr., Knopman DS, Jagust WJ, Shaw LM, Aisen PS, Weiner MW, Petersen RC, Trojanowski JQ. 2010b. Hypothetical model of dynamic biomarkers of the Alzheimer's pathological cascade. Lancet Neurol. 9:119–128.
Jansen WJ, Ossenkoppele R, Knol DL, Tijms BM, Scheltens P, Verhey FRJ, Visser PJ, Grp ABS. 2015. Prevalence of cerebral amyloid pathology in persons without dementia a meta-analysis. Jama-J Am Med Assoc. 313:1924–1938.
Jockwitz C, Caspers S, Lux S, Jutten K, Schleicher A, Eickhoff SB, Amunts K, Zilles K. 2017. Age- and function-related regional changes in cortical folding of the default mode network in older adults. Brain Struct Funct. 222:83–99.
Kelley WM, Miezin FM, McDermott KB, Buckner RL, Raichle ME, Cohen NJ, Ollinger JM, Akbudak E, Conturo TE, Snyder AZ, et al. 1998. Hemispheric specialization in human dorsal frontal cortex and medial temporal lobe for verbal and nonverbal memory encoding. Neuron. 20:927–936.
Kriegeskorte N, Goebel R, Bandettini P. 2006. Information-based functional brain mapping. Proc Natl Acad Sci U S A. 103: 3863–3868.
Lin F, Ren P, Mapstone M, Meyers SP, Porsteinsson A, Baran TM, Alzheimer's Disease Neuroimaging Initiative. 2017a. The cingulate cortex of older adults with excellent memory capacity. Cortex. 86:83–92.
Lin F, Wang X, Wu R, Rebok GW, Chapman BP, Alzheimer's Disease Neuroimaging Initiative. 2017b. Identification of successful cognitive aging in the Alzheimer's disease neuroimaging initiative study. J Alzheimers Dis. 59:101–111.
Lindenberger U. 2014. Human cognitive aging: corriger la fortune? Science. 346:572–578.
Mapstone M, Lin F, Nalls MA, Cheema AK, Singleton AB, Fiandaca MS, Federoff HJ. 2016. What success can teach us about failure: the plasma metabolome of older adults with superior memory and lessons for Alzheimer's disease. Neurobiol Aging. 51:148–155.
Mitchell TM, Hutchinson R, Niculescu RS, Pereira F, Wang XR, Just M, Newman S. 2004. Learning to decode cognitive states from brain images. Mach Learn. 57:145–175.
Nichols TE, Holmes AP. 2002. Nonparametric permutation tests for functional neuroimaging: a primer with examples. Hum Brain Mapp. 15:1–25.
Nyberg L, Lovden M, Riklund K, Lindenberger U, Backman L. 2012. Memory aging and brain maintenance. Trends Cogn Sci. 16:292–305.
Park DC, Reuter-Lorenz P. 2009. The adaptive brain: aging and neurocognitive scaffolding. Annu Rev Psychol. 60:173–196.
Pereira F, Mitchell T, Botvinick M. 2009. Machine learning classifiers and fMRI: a tutorial overview. Neuroimage. 45:S199–S209.
Persson J, Pudas S, Lind J, Kauppi K, Nilsson LG, Nyberg L. 2012. Longitudinal structure-function correlates in elderly reveal MTL dysfunction with cognitive decline. Cereb Cortex. 22: 2297–2304.
Pudas S, Persson J, Josefsson M, de Luna X, Nilsson LG, Nyberg L. 2013. Brain characteristics of individuals resisting age-related cognitive decline over two decades. J Neurosci. 33: 8668–8677.
Ren P, Lo RY, Chapman BP, Mapstone M, Porsteinsson A, Lin F, Alzheimer's Disease Neuroimaging Initiative. 2016. Longitudinal alteration of intrinsic brain activity in the striatum in mild cognitive impairment. J Alzheimers Dis. 54:69–78.

Reuter-Lorenz PA, Park DC. 2010. Human neuroscience and the aging mind: a new look at old problems. J Gerontol B Psychol Sci Soc Sci. 65:405–415.

Rogalski EJ, Gefen T, Shi J, Samimi M, Bigio E, Weintraub S, Geula C, Mesulam MM. 2013. Youthful memory capacity in old brains: anatomic and genetic clues from the Northwestern SuperAging Project. J Cogn Neurosci. 25:29–36.

Ronnlund M, Nyberg L, Backman L, Nilsson LG. 2005. Stability, growth, and decline in adult life span development of declarative memory: cross-sectional and longitudinal data from a population-based study. Psychol Aging. 20:3–18.

Rosano C, Aizenstein HJ, Newman AB, Venkatraman V, Harris T, Ding JZ, Satterfield S, Yaffe K, Study HA. 2012. Neuroimaging differences between older adults with maintained versus declining cognition over a 10-year period. Neuroimage. 62: 307–313.

Rossetti HC, Lacritz LH, Cullum CM, Weiner MF. 2011. Normative data for the Montreal Cognitive Assessment (MoCA) in a population-based sample. Neurology. 77:1272–1275.

Salat DH, Kaye JA, Janowsky JS. 2002. Greater orbital prefrontal volume selectively predicts worse working memory performance in older adults. Cereb Cortex. 12:494–505.

Salthouse TA. 2009. When does age-related cognitive decline begin? Neurobiol Aging. 30:507–514.

Scarmeas N, Zarahn E, Anderson KE, Honig LS, Park A, Hilton J, Flynn J, Sackeim HA, Stern Y. 2004. Cognitive reserve-mediated modulation of positron emission tomographic activations during memory tasks in Alzheimer disease. Arch Neurol. 61:73–78.

Schulz R, Heckhausen J. 1996. A life span model of successful aging. Am Psychol. 51:702–714.

Shulman KI. 2000. Clock-drawing: is it the ideal cognitive screening test? Int J Geriatr Psychiatry. 15:548–561.

Song XW, Dong ZY, Long XY, Li SF, Zuo XN, Zhu CZ, He Y, Yan CG, Zang YF. 2011. REST: a toolkit for resting-state functional magnetic resonance imaging data processing. PLoS ONE. 6:e25031.

Sorg C, Riedl V, Muhlau M, Calhoun VD, Eichele T, Laer L, Drzezga A, Forstl H, Kurz A, Zimmer C, et al. 2007. Selective changes of resting-state networks in individuals at risk for Alzheimer's disease. Proc Natl Acad Sci U S A. 104: 18760–18765.

Stern Y. 2002. What is cognitive reserve? Theory and research application of the reserve concept. J Int Neuropsychol Soc. 8: 448–460.

Stern Y, Zarahn E, Habeck C, Holtzer R, Rakitin BC, Kumar A, Flynn J, Steffener J, Brown T. 2008. A common neural network for cognitive reserve in verbal and object working memory in young but not old. Cereb Cortex. 18:959–967.

Sun FW, Stepanovic MR, Andreano J, Barrett LF, Touroutoglou A, Dickerson BC. 2016. Youthful brains in older adults: preserved neuroanatomy in the default mode and salience networks contributes to youthful memory in superaging. J Neurosci. 36:9659–9668.

Uddin LQ, Menon V, Young CB, Ryali S, Chen T, Khouzam A, Minshew NJ, Hardan AY. 2011. Multivariate searchlight classification of structural magnetic resonance imaging in children and adolescents with autism. Biol Psychiatry. 70: 833–841.

Waiter GD, Fox HC, Murray AD, Starr JM, Staff RT, Bourne VJ, Whalley LJ, Deary IJ. 2008. Is retaining the youthful functional anatomy underlying speed of information processing a signature of successful cognitive ageing? An event-related fMRI study of inspection time performance. Neuroimage. 41: 581–595.

Yan CG, Wang XD, Zuo XN, Zang YF. 2016. DPABI: data processing & analysis for (resting-state) brain imaging. Neuroinformatics. 14:339–351.

Zang YF, He Y, Zhu CZ, Cao QJ, Sui MQ, Liang M, Tian LX, Jiang TZ, Wang YF. 2007. Altered baseline brain activity in children with ADHD revealed by resting-state functional MRI. Brain Dev. 29:83–91.

Zimmerman ME, Brickman AM, Pau RH, Grieve SM, Tate DF, Gunstad J, Cohen RA, Aloia MS, Williams LM, Clark CR, et al. 2006. The relationship between frontal gray matter volume and cognition varies across the healthy adult lifespan. Am J Geriat Psychiatry. 14:823–833.

Zuo XN, Di Martino A, Kelly C, Shehzad ZE, Gee DG, Klein DF, Castellanos FX, Biswal BB, Milham MP. 2010. The oscillating brain: complex and reliable. Neuroimage. 49:1432–1445.